The Astronomical Journal, 153:266 (8pp), 2017 June https://doi.org/10.3847/1538-3881/aa6ea8

A Dark Asteroid Family in the Phocaea Region

Bojan Novaković[1], Georgios Tsirvoulis[2], Mikael Granvik[3], and Ana Todović[1]
[1] Department of Astronomy, Faculty of Mathematics, University of Belgrade, Studentski trg 16, 11000 Belgrade, Serbia; bojan@matf.bg.ac.rs
[2] Astronomical Observatory, Volgina 7, 11060 Belgrade 38, Serbia
[3] Department of Physics, P.O. Box 64, 00014 University of Helsinki, Finland
Received 2017 February 6; revised 2017 April 18; accepted 2017 April 19; published 2017 May 25

Abstract

We report the discovery of a new asteroid family among the dark asteroids residing in the Phocaea region the Tamara family. We make use of available physical data to separate asteroids in the region according to their surface reflectance properties, and establish the membership of the family. We determine the slope of the cumulative magnitude distribution of the family, and find it to be significantly steeper than the corresponding slope of all the asteroids in the Phocaea region. This implies that subkilometer dark Phocaeas are comparable in number to bright *S*-type objects, shedding light on an entirely new aspect of the composition of small Phocaea asteroids. We then use the Yarkovsky V-shape based method and estimate the age of the family to be 264 ± 43 Myr. Finally, we carry out numerical simulations of the dynamical evolution of the Tamara family. The results suggest that up to 50 Tamara members with absolute magnitude $H < 19.4$ may currently be found in the near-Earth region. Despite their relatively small number in the near-Earth space, the rate of Earth impacts by small, dark Phocaeas is non-negligible.

Key words: celestial mechanics – minor planets, asteroids: general

Supporting material: machine-readable table

1. Introduction

Understanding the structure and past evolution of the asteroid families in the inner asteroid belt are important for constraining the history and evolution of the belt, as well as the delivery of asteroids to the near-Earth region (Bottke et al. 2015; Granvik et al. 2017).

The Phocaea region is a high-orbital-inclination part of the inner asteroid belt, which is separated from the low-inclination asteroids by the ν_6 secular resonance. The region has dynamical boundaries from all sides but one, making it almost completely detached from the rest of the asteroid belt (Knežević & Milani 2003; Michtchenko et al. 2010).

Most of the Phocaeas[4] are classified as *S*-type asteroids (Carvano et al. 2001), typical for objects in the inner asteroid belt. Still, the relative mass contribution of each taxonomic class changes with size in each part of the asteroid belt (DeMeo & Carry 2014). The most obvious correlation is an increase of *C*-type objects as size decreases in the inner belt. Nevertheless, as far as the total number of asteroids that belong to a specific spectral type is concerned, the Phocaea region has been thought to be dominated by bright, *S*-type objects (Carvano et al. 2010; Masiero et al. 2011).

A large fraction of asteroids from the Phocaea region belong to the Phocaea collisional family (e.g., Milani et al. 2014), estimated to be about 1.2 Gyr old (Milani et al. 2017). The possible existence of other families inside this region has been discussed by several authors (Gil-Hutton 2006; Carruba 2009; Novaković et al. 2011; Masiero et al. 2013) who proposed several candidate groups that might be collisional families. Still, no family formed by a break-up of a dark carbonaceous parent body has been proposed to exist in the Phocaea region. However, as we show later in this paper, there are strong indications that such a family exists. For this reason, we focused on the population of dark (*C*-type) asteroids located in the region, and searched for potential tracers of a collisional family among these objects.

[4] We use term *Phocaeas* to refer to all asteroids from the Phocaea region, while possible additional restrictions are always explicitly mentioned.

2. Dark Phocaea Asteroids: Identification and Search for a Family

There are currently 4072 known numbered and multi-opposition asteroids in the Phocaea region.[5] Using physical data obtained by the *Wide-field Infrared Survey Explorer* (*WISE*; Masiero et al. 2011), we found that the region consists mostly of bright asteroids (∼73%) with albedos higher than 0.1.

However, the albedo distribution shows a clear separation between dark and bright asteroids (Figure 1). It is roughly the sum of two separated Gaussians, and the spreading of the low-albedo part is narrower than what we usually observe across the asteroid belt. This suggests the possible existence of a dark asteroid family.

The number density of dark asteroids in the region is far lower than the total number density, making the possible dark family totally indistinguishable if one looks at the whole asteroid population. The only way to study this family is to consider solely dark asteroids.[6]

2.1. The Identification of Dark Asteroids

The next step in our study was to obtain a catalog of dark asteroids in the region. Following Walsh et al. (2013), we

[5] Data obtained from the AstDyS service (hamilton.dm.unipi.it/astdys/). We define the Phocaea region using the following ranges in proper orbital elements: $2.1 < a_p < 2.5$ au, $0.0 < e_p < 0.4$, and $0.3 < \sin(i_p) < 0.5$.

[6] A similar effort was done by Masiero et al. (2013), who studied separately the low and high albedo asteroids across the main belt. However, they failed to identify this group due to the significant overlap between their two albedo populations.

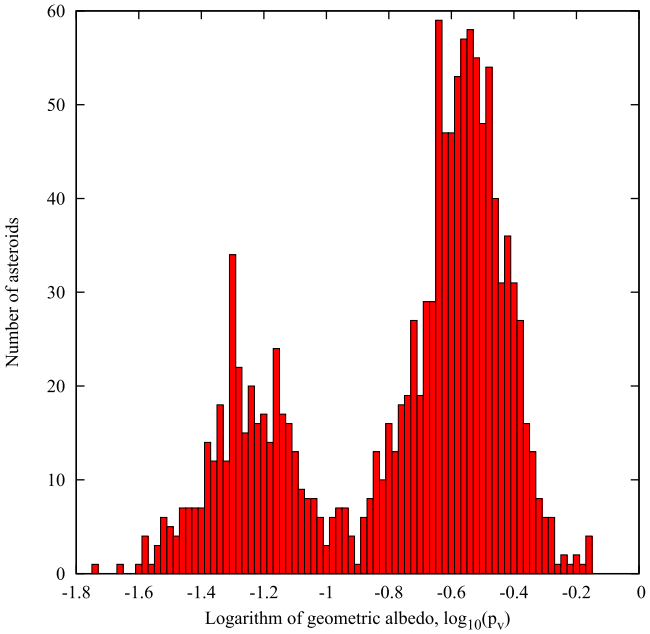

Figure 1. Geometric albedo distribution of asteroids in the Phocaea region. The presence of two distinct sub-populations is apparent. The left and right peak in the distribution represent dark and bright objects respectively.

worked with objects with geometric albedos p_v below 0.1. The *WISE* data provide albedos for 1280 out of the 4072 asteroids in the region, and of those 1280 we found 348 dark ones. In an effort to expand this catalog, we selected, in a similar manner, dark asteroids as identified by the AKARI (Usui et al. 2013), and the *Infrared Astronomical Satellite* (IRAS) (Tedesco et al. 2002) surveys, where we found 41 and 12 low-albedo asteroids, respectively.

We also made use of the MOVIS catalog (Popescu et al. 2016), which uses VISTA colors in order to distinguish between *C*- and *S*-complex asteroids. According to Popescu et al. (2016), the (*Y*–*J*) versus (*Y*–*Ks*) color space provides the largest separation between the two complexes, the separatrix being the line $(Y-J) = 0.338^{\pm 0.027} \cdot (Y-Ks) + 0.075^{\pm 0.02}$. Therefore, we considered as *C*-type those asteroids whose entire 1σ error bar lies below this line. This way we obtained eight dark asteroids.

Finally, we extracted dark asteroids as characterized by Carvano et al. (2010) using the Sloan Digital Sky Survey (SDSS) data (Ivezić et al. 2001). There are 76 objects classified as either *C*- or *D*-type, but for the purpose of this work we used only 16 asteroids, which have a >50% probability to belong to the one of specified taxonomic types.

In this way, we identified 381 dark objects, and after removing 5 asteroids with contradictory albedos,[7] we obtained the catalog of dark Phocaeas containing 376 objects.

The dark component of this population has a non-uniform number density in the proper elements space (Figure 2), suggesting the presence of an asteroid family.

2.2. The Search for a Family

We performed a Hierarchical Clustering analysis (Zappala et al. 1990) on the catalog of dark objects to obtain the membership of the new family. We selected the asteroid (326) Tamara as the starting body, because it is potentially the largest member of the family, and increased the cutoff velocity from 100 to 600 m s^{-1} in steps of 5 m s^{-1}. The cutoff velocities are overall higher than what we usually encounter in similar studies, but the fact that we use only dark asteroids whose number densities are low in this region justifies these values.[8]

The result is shown in the bottom-left panel of Figure 2. The family membership is defined at the cutoff of 350 m s^{-1}, because this value belongs to the well defined plateau visible in Figure 2 (see, e.g., Novaković et al. 2011 for details on this methodology). The nominal cutoff corresponds to 226 members (Table 1), which equals about 60% of all dark asteroids found in the region. This membership includes asteroid (326) Tamara,[9] as the largest family member. Therefore, we named this group the Tamara family.

3. The Tamara Asteroid Family

3.1. Size and Escape Velocity of the Parent Body

To gain more insight into the family and its evolution, it is necessary to estimate the escape velocity from the parent body as well as the size of its parent body as these two are known to be related (Sachse et al. 2015).

A simple way to estimate the size of the parent body is to sum up the diameters of the largest and the third largest family members (Tanga et al. 1999). In this case, these are the asteroids (326) Tamara and (1942) Jablunka, with diameters of 89.4 and 16.7 km, respectively. This gives a diameter for the parent body of 106.1 km. Consequently, the largest remnant contains about 60% of the total mass of the family, indicating that the Tamara family was formed in a typical catastrophic collision.

Assuming a density of 1300 kg m^{-3}, typical for *C*-type asteroids (Carry 2012), we estimate the escape velocity from the parent body to be 45 m s^{-1}.

3.2. The Cumulative Distribution of the Absolute Magnitudes

Another important characteristic of the family is its cumulative magnitude frequency distribution (CMFD), which should follow a power law of the form $N(<H) \approx 10^{\alpha H}$. The slope parameter α can be estimated by numerically fitting the CMFD of the family members in a specific range of absolute magnitude. Here we performed this fitting in the 14.5–16.5 range, and found that $\alpha = 0.42 \pm 0.02$. This is illustrated in the bottom-right panel of Figure 2. The relatively shallow slope suggests that the Tamara family is probably not young because the young families are typically characterized by somewhat steeper slopes (Vokrouhlický et al. 2006).

It is interesting to compare the slope of the family to that of Phocaeas, in general, to estimate how large the fraction of the family members is among small Phocaeas. To this end, we derived the slope of the CMFD of all Phocaeas in the same magnitude range as for the Tamara family, i.e., 14.5–16.5 mag,

[7] In our sample asteroids, (587), (2105), (4899), (8356), and (74749) have albedo determined from two different surveys but the results are inconsistent.

[8] Nesvorný et al. (2015) used 150 m s^{-1} to determine the membership of the Phocaea family within the whole population of Phocaeas. Because known dark asteroids account for about 9% of all Phocaeas (376/4072), but occupy almost the same volume in the orbital space, a reasonable value to define the dark family should be about $\sqrt{11}$ times larger than the one used for the Phocaea family. This is why we select 350 m s^{-1} as the nominal cutoff, rather than a value from the first plateau seen around 250 m s^{-1}.

[9] Despite being linked in some classifications to the Phocaea family, with an albedo of 0.040 ± 0.002 (Usui et al. 2013), the asteroid Tamara obviously does not belong to this group.

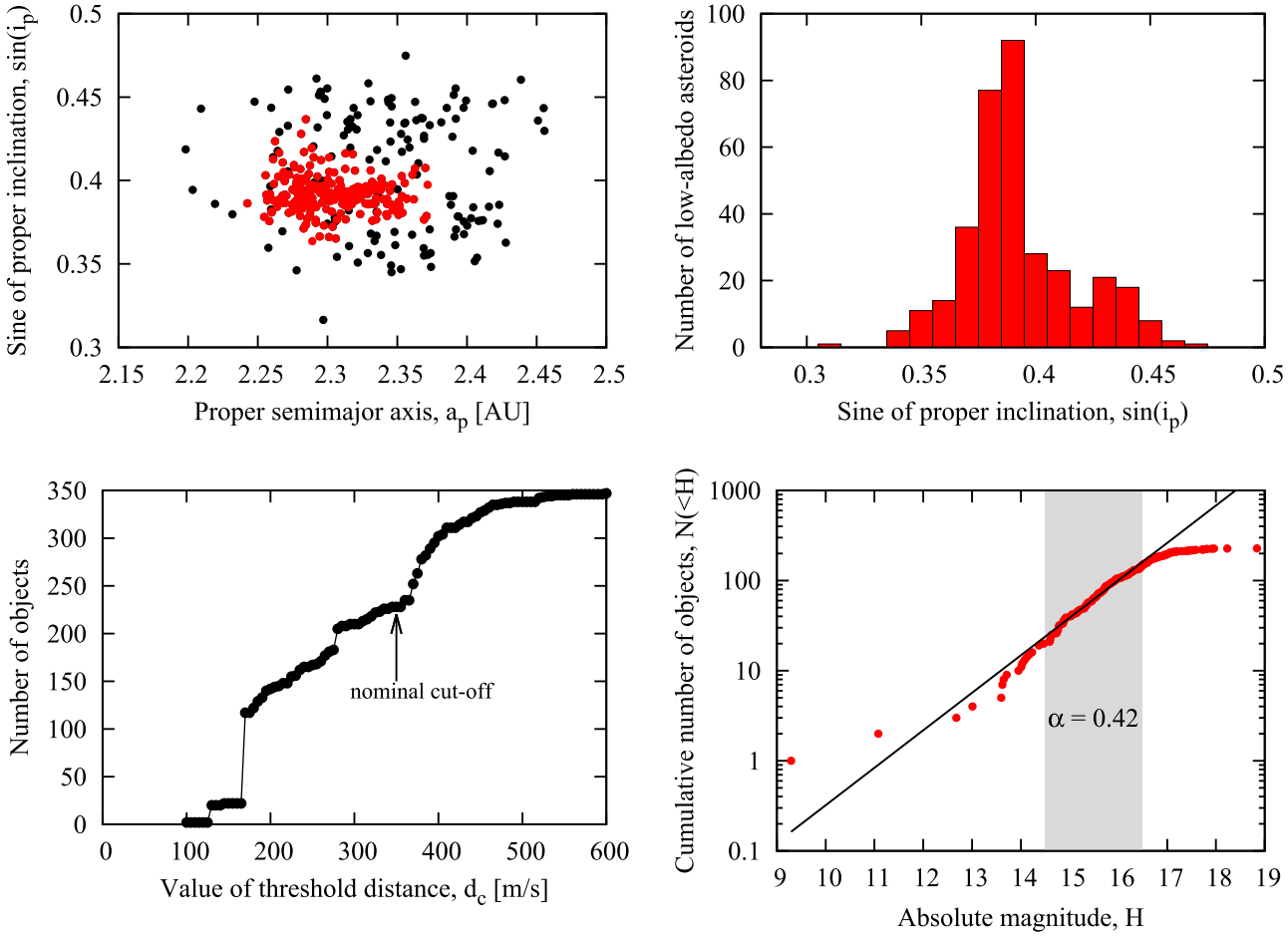

Figure 2. Properties of low-albedo asteroids in the Phocaea region. Top-left panel: proper semimajor axis vs. sine of proper inclination projection of the dark asteroids in the Phocaea region (black dots), and Tamara family members (red dots). Top-right panel: histogram of orbital inclinations of dark Phocaeas. Bottom-left panel: number of asteroids associated with the family as a function of cutoff velocity. Bottom-right panel: the cumulative magnitude distribution of the Tamara family (red dots), and its the best-fitting line (black solid line). The dashed area indicates the interval used for the fitting.

and obtained $\alpha = 0.28 \pm 0.01$. The slope is significantly shallower than the one derived for the Tamara family. This is somewhat expected because the population of Phocaeas is dominated by the very old Phocaea collisional family.

Finally, assuming that the derived slopes of the CMFDs are valid for magnitudes larger than those used to compute them, we predict the number of all Phocaeas and of Tamara family members to be about 24,500 and 4,200, respectively, for $17 < H < 20$. That is, about 17% of all Phocaeas should be members of the Tamara family. The fraction of family members is even larger for magnitudes $H > 20$, meaning that among the small Phocaeas there may be as many dark asteroids as bright ones. See Section 4.2.1 for an additional discussion on this.

3.3. Age of the Family

We used the "V-shape" method, which is based on the size-dependent secular drift in semimajor axis induced by the Yarkovsky effect, to estimate the age of the new family (Vokrouhlický et al. 2006; Spoto et al. 2015). The existence of such a structure could also be used to verify the collisional origin of the group (Walsh et al. 2013; Bolin et al. 2017).

From the available physical data, we computed the mean albedo for family members to be $\bar{p}_v = 0.059 \pm 0.016$. Using this value, we can convert absolute magnitudes to diameters[10] and plot the semimajor axis versus the inverse of the diameter (a_p, $1/D$), as shown in Figure 3. The V-shape structure is clearly visible, providing evidence that the Tamara family is a real collisional family.

In order to estimate the age of the Tamara family, we employed a method very similar to the one proposed by Spoto et al. (2015). First, we divided the family into left (inner) and right (outer) sides with respect to the barycenter. Then we divided the $1/D$-axis in intervals containing equal numbers of asteroids, and identified the objects with the minimum/maximum value of a_p for each interval on the left/right side.

This data was used to perform a two-step fitting procedure to determine the slopes of the distribution of the family members in the (a_p, $1/D$) plane. We fit the lines through these furthest objects on both sides in the (a_p, $1/D$) plane. Then the objects located more than 0.045 below the lines (in $1/D$) were removed from the calculation as outliers. Additionally, on the left (inner) side, we also removed a single object with $a_p < 2.25$ au, because its semimajor axis may be affected by the 7/2

[10] We estimated diameters in this way only for the members lacking a direct estimate. This is because the infrared surveys measure emitted flux, that is then used to derive the diameters. As a result, the diameters obtained are more reliable than the albedos (Mainzer et al. 2011).

Table 1
List of the Tamara Family Members

Name[a]	H[b]	a[c]	e[d]	sin(i)[e]	n[f]	g[g]	s[h]
326	9.29	2.3175924	0.2033926	0.3943312	102.025399	16.665155	−34.712405
1342	11.08	2.2890380	0.2100640	0.3636707	103.940145	19.330543	−35.240851
1942	13.01	2.3183473	0.2066104	0.3947821	101.974747	16.658029	−34.847479
7703	14.59	2.3059156	0.2007934	0.3651971	102.800888	19.380284	−35.289497
16635	14.01	2.2982526	0.2211551	0.3972546	103.316078	16.412431	−34.883484
27851	13.62	2.3102585	0.1877882	0.3897257	102.511556	16.847250	−33.895959
29475	13.60	2.3566943	0.2122856	0.3890748	99.496381	17.843176	−36.794154
31359	14.63	2.2724503	0.2004740	0.4035276	105.081185	15.310253	−32.856066

Notes.
[a] Asteroid name or designation.
[b] Absolute magnitude (mag).
[c] Proper semimajor axis (au).
[d] Proper eccentricity.
[e] Sine of proper inclination.
[f] Mean motion (deg/yr).
[g] Proper frequency of node (arcsec/yr).
[h] Proper frequency of perihelion (arcsec/yr).
(This table is available in its entirety in machine-readable form.)

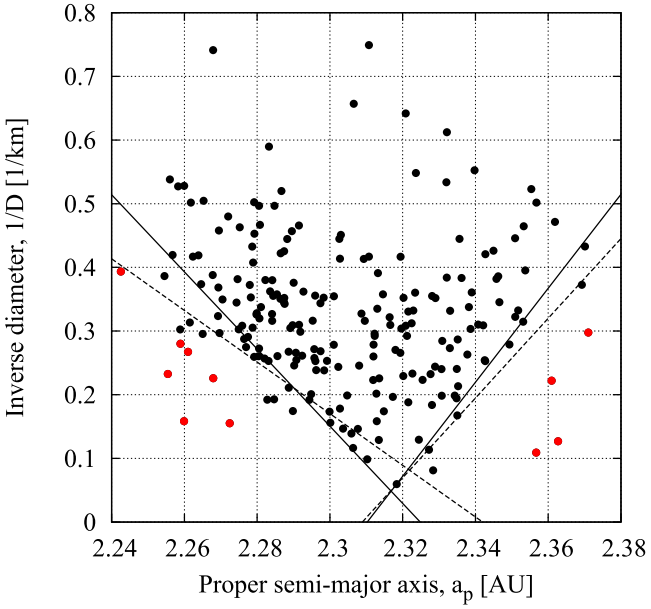

Figure 3. Proper semimajor axis vs. the inverse diameter for the members of the family. The dashed and solid lines correspond to the initial and final V-shape fit, respectively. Red dots mark the outliers removed from the fit after the first iteration.

resonance with Jupiter (Milić Žitnik & Novaković 2015). After removing these objects, we again fitted the members with the minimum/maximum value of a_p for each interval and obtained the slopes of the V-shape (Figure 3).

The method of family age estimation based on V-shapes requires a Yarkovsky calibration, that is, an estimate for the maximum value of the Yarkovsky driven secular drift $(da/dt)_{\max}$ for a hypothetical family member of diameter $D = 1$ km (Milani et al. 2014). The value of $(da/dt)_{\max}$ is determined using a model of the Yarkovsky effect and assuming thermal parameters appropriate for regolith-covered C-type objects (Vokrouhlický et al. 2015). We adopted $\rho_s = \rho_b = 1300\,\mathrm{kg\,m^{-3}}$ for the surface and bulk densities (Carry 2012), $\Gamma = 250\,\mathrm{J\,m^{-2}\,s^{-1/2}\,K^{-1}}$ for the surface thermal inertia (Delbó & Tanga 2009), and $\epsilon = 0.95$ for the thermal emissivity parameter. With these parameters, we estimated that the maximum drift speed $(da/dt)_{\max}$ is about 5.3×10^{-4} au/Myr for a body with $D = 1$ km.

Finally, using the inverse slopes and the adopted Yarkovsky calibration, we estimated the age of the family to be 264 ± 43 Myr.

4. Dynamical Evolution of the Tamara Family

Numerous gravitational and non-gravitational perturbations constantly modify asteroid orbits (e.g., Nesvorný et al. 2015). Also the group of asteroids forming an asteroid family evolves in time, being gradually dispersed by mean motion or secular resonances (Novaković 2010; Novaković et al. 2015; Carruba et al. 2016), close encounters with planets or massive asteroids (Carruba et al. 2003; Novaković et al. 2010) and the Yarkovsky effect (Bottke et al. 2001; Vokrouhlický et al. 2015). Thus, it is of great importance to reconstruct the dynamical evolution of the family because this may help, for example, to set additional constrains about its age, or to evaluate the possible leakage from the family toward the near-Earth region.

4.1. Dynamical Model and Initial Conditions

To simulate the dynamical evolution of the Tamara family, we performed a set of numerical integrations. For this purpose, we employed the *ORBIT9* integrator embedded in the multi-purpose *OrbFit* package.[11] The dynamical model includes the gravitational effects of the Sun and seven major planets, from Venus to Neptune, and also accounts for the Yarkovsky effect.

Our simulations follow the long-term orbital evolution of test particles initially distributed randomly inside an ellipse determined by the Gauss equations. This ellipse corresponds to the dispersion of the Tamara family members immediately after the breakup event, assuming an isotropic ejection of the fragments from the parent body (Morbidelli et al. 1995; Nesvorný et al. 2002). The center of the ellipse coincides with a

[11] Available from http://adams.dm.unipi.it/orbfit/.

position of asteroid (323) Tamara in the space of osculating semimajor axis, eccentricity, and inclination. At the beginning of the integration, we set the three angular elements (nodal longitude, argument of perihelion, and mean anomaly) for all test particles equal to the corresponding elements of asteroid Tamara. This ensures that the Gaussian ellipse defined in the space of osculating elements corresponds to the position of the Tamara family in the proper element space.

The ellipse is obtained assuming a relatively conservative velocity change of 20 m s^{-1} (see, e.g., Carruba & Nesvorný 2016, for typical ejection velocities of asteroid families). Our analysis presented is not very sensitive to this choice. In particular, estimation of the flux toward the NEO region is not significantly affected by the initial size of the family. A larger initial velocity field would, however, cause fragments to reach the NEO region somewhat earlier than in the case studied here.

For simplicity, the Yarkovsky effect is approximated as a pure along-track acceleration, inducing on average the same semimajor axis drift speed da/dt as predicted from theory.

Since the Yarkovsky effect scales as $\propto 1/D$, the particle sizes are used to calculate the corresponding value of (da/dt) for each particle, by scaling from the reference value derived for a $D = 1$ km object (see Section 3.3). Assuming an isotropic distribution of spin axes in space, to each particle we randomly assign a value from the $\pm(da/dt)$ interval.

To obtain the sizes of the test particles, we first assign them absolute magnitude values that follow a CMFD with the same slope as that of the real family (see Section 3.2), and then convert them to diameters.

4.2. The Dynamical Evolution: Outcome of Numerical Simulations

The dynamical evolution of the family in the proper elements space was simulated over 350 Myr, i.e., about 90 Myr longer than the estimated age of the family. The results obtained after 250–300 Myr of evolution very nearly matched the current spreading of the family in the space of proper orbital elements (Figures 4 and 5). This provides independent evidence that the Tamara family is indeed the evolutionary outcome of a fragmentation event in this region.

However, a small part of the low-inclination region of the family was not fully reproduced—specifically around a proper semimajor axis of 2.3 au (see Figure 4). There are several family members located at a sine of proper inclination smaller than 0.37, but this location was not reached by the test particles. Therefore, we speculate that these objects might have been injected there due to an anisotropic ejection velocity field, or, they may not be real family members, but interlopers associated to the family as a result of the chaining effect, a well known drawback of the HCM (see, e.g., Novaković et al. 2012).

Being located at the inner edge of the main asteroid belt, the Tamara family is potentially an important source of low-albedo near-Earth objects (NEOs). Since the current members of the family, being large enough, are still far from the resonances capable of transporting asteroids close to Earth, only smaller members, which drift faster, could have contributed to the NEO flux. Therefore, we focus here on objects with $17 < H < 19.35$ mag.

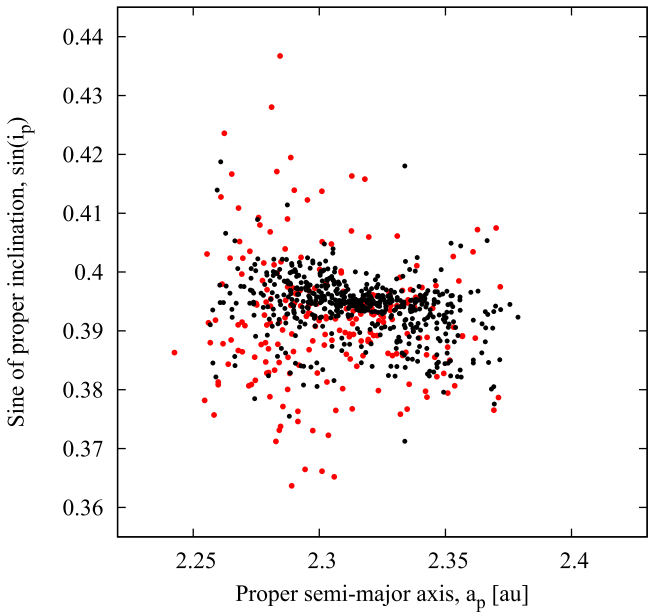

Figure 4. Real and simulated Tamara family in the space of proper orbital semimajor axis vs. sine of proper orbital inclination. The red points represent the real family members, while the black points show the distribution of the test particles after 260 Myr of the evolution. Note that only test particles covering the same size range as the real family members are shown.

4.2.1. The Flux toward the NEO Region

In order to estimate the number of NEOs originating from the family, we analyzed the outputs of the integrations, looking for those particles that at some point over the covered time span, reached perihelion distances below 1.3 au. We determined the total number of objects reaching the near-Earth region as a function of time, as well as the number of members settled in the NEO space at any specific point in time.

Based on the CMFD slope α of the Tamara family, we estimated that there should be 2,280 real members with $17 < H < 19.35$ mag. We used this number of test particles to study the flux toward the NEO region because they should represent the real family in the considered range of magnitudes.

The results are shown in Figure 6. In this figure, the bold line shows the cumulative number of particles reaching perihelion distances $q < 1.3$ au. It seems that the first family members became NEOs about 100 Myr after the family formation event, with about 800 test particles in total reaching this area during the subsequent 250 Myr of the simulation. Therefore, the cumulative number is increasing almost linearly with time, suggesting that the flux from the family is about three test particles per megayear. Given the estimated age of the Tamara family of 264 Myr, about 500 of its members with $17 < H < 19.35$ should have reached NEO space so far.

In Figure 6, the gray points represent the number of the Tamara family members residing in the near-Earth region at any specific point in time. This result suggests that up to 50 objects from the family may be found in the region of terrestrial planets. Focusing on the time interval between 221 and 307 Myr of the evolution (lower and upper limit of the age of the family), we found that currently there should be 31 ± 6 family members in the NEO space. Taking into account other possible uncertainties, such as the uncertainty of the MFD slope, we found that the maximum possible contribution of the family is about 50 asteroids.

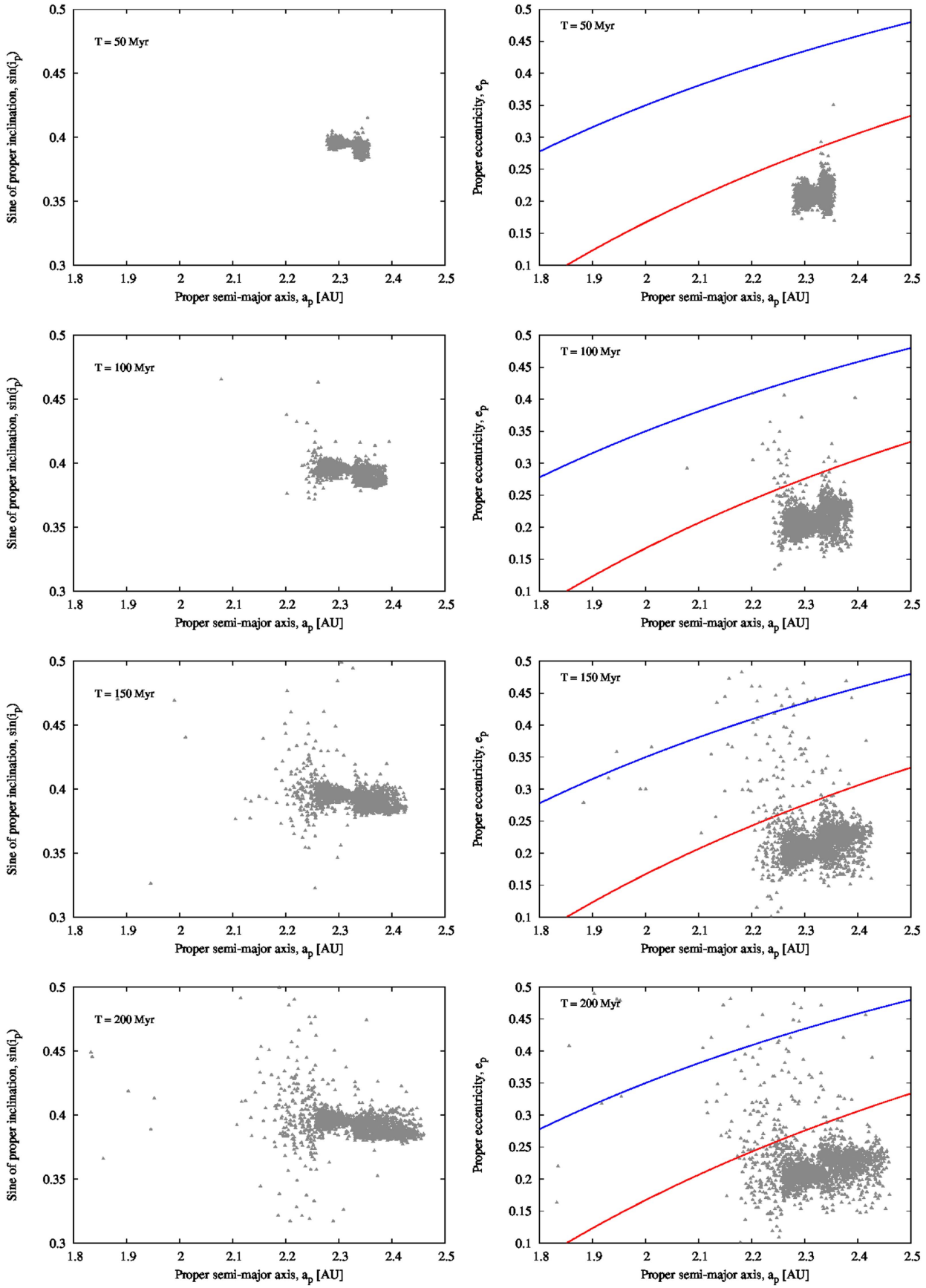

Figure 5. Evolution of the Tamara family in the space of proper orbital elements. The four panels in each column show the distribution of the test particles after 50, 100, 150, and 200 Myr (from top to bottom) of evolution. The red and blue lines mark perihelion distances q of 1.666, 1.3 au, used to define populations of Mars-crossers and near-Earth objects, respectively.

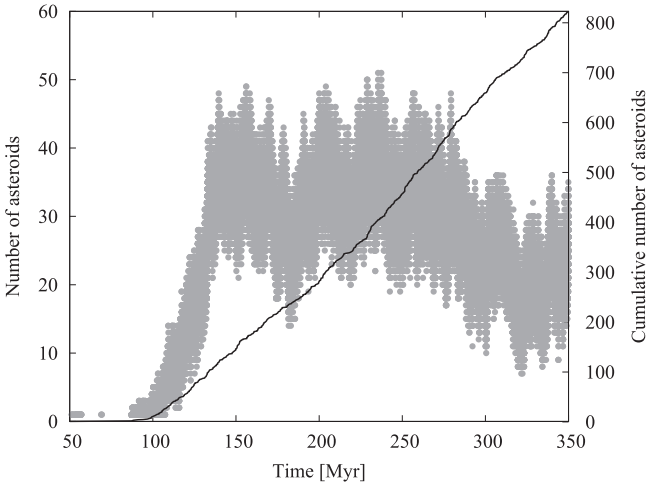

Figure 6. Tamara asteroid family as a source of NEOs. The cumulative number of test particles entering the near-Earth region (bold curve), and the total number of members residing in the near-Earth region at any specific point in time (gray dots).

It is interesting to compare this number with the recent model of NEO populations by Granvik et al. (2016). These authors found that, in the magnitude range we considered here, there should be about 250 Phocaeas residing in the NEOs space. Hence, about 13% of all NEOs coming from the Phocaea region should originate in the newly discovered family, with an upper limit of about 20%. Moreover, having a somewhat steeper slope of the cumulative magnitude distribution than the rest of the Phocaeas, the contribution of the Tamara family is likely to be even larger for smaller objects with $D < 700$ m.

Moreover, the Granvik et al. (2016, 2017) NEO model predicts that the number of NEOs with $17 < H < 22$ originating in the Phocaea region should be about 670, which represents about 3% of the entire NEO population. This is comparable to the fraction of objects originating in the outer main belt with $a > 3$ au (3.5%) and the Jupiter-family comets (2%). The rate of Earth impacts by NEOs originating in the Phocaea region is similar to that for NEOs from the outer asteroid belt but an order of magnitude greater compared to NEOs originating in the Jupiter-family comet population (M. Granvik et al. 2017, in preparation). The Tamara family is thus an important source for carbonaceous Earth impactors.

5. Summary and Conclusions

We present here a detailed study of a population of dark asteroids in the Phocaea region, and found compelling evidence for the existence of a new asteroid family within this subpopulation of Phocaeas.

We have determined the slope of the cumulative magnitude distribution of the family, and compared it with the corresponding slope for all asteroids in the Phocaea region. This brought us to the conclusion that for subkilometer Phocaeas, the number of dark *C*-type asteroids is comparable to the number of bright *S*-type objects, questioning the well-established view on this population being almost entirely composed of rocky asteroids.

Furthermore, based on the standard V-shape method, we estimated this family to be 264 ± 43 Myr old.

Finally, extensive numerical simulations were carried out allowing us to estimate that 31 ± 6 family members with $H \in [17, 19.35]$, should exist in the NEO space.

Despite their relatively small number in the near-Earth space, the impact rate from small, dark Phocaeas is non-negligible and may be an important source for dark meteorites whose parent bodies have $17 < H < 22$. We hypothesize that the peak in the distribution of meteor streams (Brown et al. 2010) at about 35–40 degrees (see Figure 14S in Granvik et al. 2016) may partly be produced by parent asteroids coming from the Phocaea region.

This work has been supported by the European Union [FP7/2007–2013], project: STARDUST-The Asteroid and Space Debris Network. B.N. also acknowledges support by the Ministry of Education, Science and Technological Development of the Republic of Serbia, Project 176011. M.G. was funded by grant #1299543 from the Academy of Finland. Numerical simulations were run on the PARADOX-III cluster hosted by the Scientific Computing Laboratory of the Institute of Physics Belgrade.

References

Bolin, B. T., Delbo, M., Morbidelli, A., & Walsh, K. J. 2017, Icar, 282, 290
Bottke, W. F., Vokrouhlický, D., Brož, M., Nesvorný, D., & Morbidelli, A. 2001, Sci, 294, 1693
Bottke, W. F., Vokrouhlický, D., Walsh, K. J., et al. 2015, Icar, 247, 191
Brown, P., Wong, D. K., Weryk, R. J., & Wiegert, P. 2010, Icar, 207, 66
Carruba, V. 2009, MNRAS, 398, 1512
Carruba, V., Burns, J. A., Bottke, W., & Nesvorný, D. 2003, Icar, 162, 308
Carruba, V., Domingos, R. C., Aljbaae, S., & Huaman, M. 2016, MNRAS, 463, 705
Carruba, V., & Nesvorný, D. 2016, MNRAS, 457, 1332
Carry, B. 2012, P&SS, 73, 98
Carvano, J. M., Hasselmann, P. H., Lazzaro, D., & Mothé-Diniz, T. 2010, A&A, 510, A43
Carvano, J. M., Lazzaro, D., Mothé-Diniz, T., Angeli, C. A., & Florczak, M. 2001, Icar, 149, 173
Delbó, M., & Tanga, P. 2009, P&SS, 57, 259
DeMeo, F. E., & Carry, B. 2014, Natur, 505, 629
Gil-Hutton, R. 2006, Icar, 183, 93
Granvik, M., Morbidelli, A., Jedicke, R., et al. 2016, Natur, 530, 303
Granvik, M., Morbidelli, A., Vokrouhlický, D., et al. 2017, A&A, 598, A52
Ivezić, Ž, Tabachnik, S., Rafikov, R., et al. 2001, AJ, 122, 2749
Knežević, Z., & Milani, A. 2003, A&A, 403, 1165
Mainzer, A., Bauer, J., Grav, T., et al. 2011, ApJ, 731, 53
Masiero, J. R., Mainzer, A. K., Bauer, J. M., et al. 2013, ApJ, 770, 7
Masiero, J. R., Mainzer, A. K., Grav, T., et al. 2011, ApJ, 741, 68
Michtchenko, T. A., Lazzaro, D., Carvano, J. M., & Ferraz-Mello, S. 2010, MNRAS, 401, 2499
Milani, A., Cellino, A., Knežević, Z., et al. 2014, Icar, 239, 46
Milani, A., Knežević, Z., Spoto, F., et al. 2017, Icar, 288, 240
Milić Žitnik, I., & Novaković, B. 2015, MNRAS, 451, 2109
Morbidelli, A., Zappala, V., Moons, M., Cellino, A., & Gonczi, R. 1995, Icar, 118, 132
Nesvorný, D., Bottke, W. F., Jr., Dones, L., & Levison, H. F. 2002, Natur, 417, 720
Nesvorný, D., Brož, M., & Carruba, V. 2015, in Asteroids IV, ed. P. Michel, F. E. DeMeo, & W. F. Bottke (Tucson, AZ: Univ. Arizona Press), 297
Novaković, B. 2010, MNRAS, 407, 1477
Novaković, B., Cellino, A., & Knežević, Z. 2011, Icar, 216, 69
Novaković, B., Hsieh, H. H., & Cellino, A. 2012, MNRAS, 424, 1432
Novaković, B., Maurel, C., Tsirvoulis, G., & Knežević, Z. 2015, ApJL, 807, L5
Novaković, B., Tsiganis, K., & Knežević, Z. 2010, CeMDA, 107, 35
Popescu, M., Licandro, J., Morate, D., et al. 2016, A&A, 591, A115
Sachse, M., Schmidt, J., Kempf, S., & Spahn, F. 2015, JGRE, 120, 1847
Spoto, F., Milani, A., & Knežević, Z. 2015, Icar, 257, 275
Tanga, P., Cellino, A., Michel, P., et al. 1999, Icar, 141, 65

Tedesco, E. F., Noah, P. V., Noah, M., & Price, S. D. 2002, AJ, 123, 1056
Usui, F., Kasuga, T., Hasegawa, S., et al. 2013, ApJ, 762, 56
Vokrouhlický, D., Bottke, W. F., Chesley, S. R., Scheeres, D. J., & Statler, T. S. 2015, in Asteroids IV, ed. P. Michel, F. E. DeMeo, & W. F. Bottke (Tucson, AZ: Univ. Arizona Press), 509
Vokrouhlický, D., Brož, M., Bottke, W. F., Nesvorný, D., & Morbidelli, A. 2006, Icar, 182, 118
Walsh, K. J., Delbó, M., Bottke, W. F., Vokrouhlický, D., & Lauretta, D. S. 2013, Icar, 225, 283
Zappala, V., Cellino, A., Farinella, P., & Knežević, Z. 1990, AJ, 100, 2030